Published in final edited form as:
Methods Mol Biol. 2014 ; 1117: 367–384. doi:10.1007/978-1-62703-776-1_17.

Visualization of DNA and Protein-DNA Complexes with Atomic Force Microscopy

Yuri L. Lyubchenko[1,*], **Alexander A. Gall**[2], and **Luda S. Shlyakhtenko**[1]

[1]Department of Pharmaceutical Sciences, University of Nebraska Medical Center, 986025 Nebraska Medical Center, Omaha, NE 68198-6025, USA

[2]Cepheid, 1631 220th St. SE Ste. 102, Bothell, WA 98021, USA

Abstract

This article describes sample preparation techniques for AFM imaging of DNA and protein–DNA complexes. The approach is based on chemical functionalization of the mica surface with aminopropyl silatrane (APS) to yield an APS-mica surface. This surface binds nucleic acids and nucleoprotein complexes in a wide range of ionic strengths, in the absence of divalent cations, and in a broad range of pH. The chapter describes the methodologies for the preparation of APS-mica surfaces and the preparation of samples for AFM imaging. The protocol for synthesis and purifi cation of APS is also provided. The AFM applications are illustrated with examples of images of DNA and protein–DNA complexes.

Keywords

Atomic force microscopy; AFM; mica functionalization; surface chemistry; silanes; silatranes; DNA structure and dynamics; protein-DNA complexes

1 Introduction

1.1 AFM Basics

The prototype scanning tunneling microscope (STM) instrument was conceived by Binnig and Rohrer [1, 2], an invention for which the authors were awarded the 1986 Nobel Prize in Physics. The atomic force microscope (AFM) was invented in 1986 [3], and commercial instruments became available to the biological community shortly thereafter. A schematic illustrating the principles of the AFM operation is shown in Fig. 1. A sharp stylus (AFM tip shown as a triangle) reads the profile of the sample (shown as a bumpy profile) by scanning over the sample. The tip is attached to a cantilever that works as a spring pressing the tip against the sample to reproduce the surface profile. The vertical position of the tip is measured by a laser light reflected from the cantilever to the position-sensitive photodetector (PSD). According to this scheme, no special contrasting sample is needed for AFM imaging.

[*]Corresponding author: Yuri L. Lyubchenko, Department of Pharmaceutical Sciences, University of Nebraska Medical Center, 986025 Nebraska Medical Center, Omaha, NE 68198-6025, Phone: 402-559-1971-office, ylyubchenko@unmc.edu.

Additionally, scanning can be performed in any media at ambient conditions, including physiological conditions, making AFM very valuable for biological applications.

AFM instruments include a number of important features that enable the production of high-resolution images. First, the position of the sample relative to the tip is controlled by the scanner with an accuracy of less than 1 nm. Second, the tip can be atomically sharp. Third, the displacement of the tip relative to the surface is determined with sub-nanometer accuracy. These three major features provide the foundation for AFM's capability of producing topographic images with atomic accuracy. Atomic resolution was achieved with AFM in an early paper [4] in which the atomic-scale periodicities of calcite as well as the expected relative positions of the atoms within each unit cell were obtained. This capability of achieving atomic level resolution was further exemplified by a recent publication reporting differences of 74 pm in lengths of covalent single and double bonds [5]. The authors estimate that the developed AFM methodology (the instrument operated in a noncontact mode at cryogenic temperature, 5 K) is capable of measuring the bond length difference down to 30 pm.

Figure 2 illustrates the major operating modes of AFM. The operating mode corresponding to the attraction part of the tip–sample interaction potential is termed noncontact mode (NC-AFM). After passing the minimum on the potential curve, the repulsion interaction rises steeply, achieving large positive values in a very short range of the tip–sample distances. This scanning regime is termed contact mode. In this regime, the tip strongly interacts with the surface; therefore, in the contact mode AFM does not allow for obtaining reliable and robust imaging biological samples. Importantly, damage or deformation of soft biological samples can be made by the tip during the approach or scanning process.

The alternating contact (AC) AFM mode is efficient in numerous biological applications and was initially proposed in [6]. In this mode, the AFM tip oscillates with a frequency much faster than the scanning frequency and is in contact with the sample during a short period of time. For typical AFM experiments in air, the tip oscillates with ~100 KHz, while the scanning frequency is 2–4 Hz. This mode dramatically decreases tip deformation and dragging effects. Another term for AC mode is tapping mode [7]; but the name has been trademarked by the AFM manufacturer, Veeco. Other manufacturers use AC mode or intermediate or intermittent contact mode (IC mode). Schematically, the range of operation of the AC/IC/TM mode is illustrated in Fig. 2 with a thick horizontal double arrow.

In contact mode, the tip–sample distance is maintained by measuring the deflection of the tip cantilever determined by van der Waals repulsion forces. However, the detection principle for the intermediate mode is different. In AC/IC/TM-AFM, a cantilever is deliberately vibrated at the frequency close to the cantilever resonance frequency by a piezoelectric modulator with a very small amplitude. As the tip approaches a surface, the van der Waals attractive force between the tip and the sample changes both the amplitude and the phase of the cantilever vibration [8]. These changes are monitored by a Z-servo system feedback loop to control the tip–sample distance. The ability of the AC/IC/TM mode to image biological samples gently is the primary attractive feature of this operating mode. The paragraphs

below briefly describe a few examples in which AC/IC/TM-AFM was applied to image DNA and protein–DNA complexes.

1.2 AFM for Imaging of Protein–DNA Complexes

Figure 3a shows an AFM image of supercoiled DNA with a plectonemic morphology formed by interwound DNA strands of a circular DNA molecule. The next frame (Fig. 3b) shows the complex of DNA with the site-specific binding protein SfiI, as described in refs. [9, 10]. This is a restriction enzyme that cleaves DNA when it binds two recognition sites on DNA forming a synaptic complex, as shown schematically below the image. The images contain looped complexes directly proving the existence of synaptic complexes (Mg^{2+} cations were replaced with Ca^{2+} cations to prevent DNA cleavage). Protein binding specificity was confirmed by the length measurements of multiple images. Schematic in (b) illustrates the positions of binding sites (squares) on the DNA substrate.

An intramolecular DNA triplex or H-DNA formed by homopurine–homopyrimidine (Pu·Py) tracts is a biologically important alternative DNA structure [11]. Structural studies of intramolecular triplexes are instrumental in understanding the mechanism of how H-DNA is involved in genetic processes. The challenge in imaging H-DNA is the requirement of low pH. This requirement was met in a publication [12] in which the functionalized mica approach was implemented. A high-resolution AFM image of pUC19 plasmid with a 46 bp long purine–pyrimidine repeat prepared at acidic pH is shown in Fig. 3d. A distinct feature of the molecules prepared at acidic pH is the formation of a clear kink with a short protrusion indicated by an arrow. The formation of a sharp kink is fully consistent with the model of an intramolecular DNA triplex [11, 13] shown schematically in Fig. 3c. The same technique was instrumental in detecting the H-DNA conformation in long imperfect Py–Pu inserts [14].

Figure 3d illustrates the ability of AFM to image another type of transient DNA conformation, cruciforms. Negative DNA supercoiling is required for cruciform stabilization. The cruciform appears on the AFM image as a clear-cut extrusion as indicated with an arrow. The sizes of the arms for extended extrusions are 15–20 nm, in full agreement with the expected length of the hairpins containing 53 bp (18 nm for B-helix DNA geometry). The identification of two classes of cruciforms, discovered by AFM imaging, led to the hypothesis of a novel regulatory role of cruciforms in global DNA dynamics [15]. Both alternative DNA structures, cruciforms and H-DNA, are involved in the regulation of DNA transcription; therefore, the ability of AFM to image alternative DNA structures makes AFM a very valuable tool in the field of molecular and structural genetics.

Figure 3e shows an AFM image of the complex formed by a cruciform with RuvA protein [15]. RuvA is the key protein involved in DNA homologous recombination that recognizes four-way DNA junctions, such as cruciforms. AFM confirmed this binding specificity demonstrating that after binding to the cruciform, the protein unfolds it and keeps the cruciform in unfolded conformation. Based on these findings the authors proposed a novel regulatory mechanism for DNA recombination [15].

The ability of AFM to image a large DNA assembly termed kinetoplast DNA (kDNA), in addition to individual DNA molecules, was demonstrated in [16] (*see* Fig. 3f). This natively existing large and fragile molecular assembly consists of several thousand DNA circles of approximately 2 kb (minicircles) and a few dozen much larger DNA molecules, termed macrocircles, interlocked into a network. The gentle operating capabilities of AFM, combined with appropriate sample preparation procedures, were two critical issues enabling the observation of intact fragile biological systems such as kDNA [16].

1.3 Time-Lapse AFM Imaging of Protein–DNA Complexes

One of the important features of AFM is the ability to scan samples in aqueous solutions. This mode of AFM imaging is appealing for two major reasons. First, imaging of the fully hydrated sample eliminates potential problems inherent with sample drying. Second, imaging in liquid allows for time-lapse visualization of sample dynamics and interactions. Importantly, due to AFM resolution at the nanometer scale, dynamics are observed at the nanoscale level. Various protein–DNA systems were analyzed with the time-lapse AFM that were reviewed in refs. [17–19]; see also references therein. The drawback of AFM time-lapse studies is the slow (minute-scale) data acquisition rate of a conventional AFM instrument, so most system dynamics remain undetectable. Ando's group has developed a high-speed AFM (HS-AFM) instrument operating almost 1,000 times faster and capable of acquiring data with a sub-second rate [20–22]. With this instrument, Ando's group was able to visualize the dynamics of individual myosin molecules with a 100 ms temporal resolution [21, 22]. HS-AFM was instrumental in the analysis, performed by our group and others, of various protein–DNA complexes [23–27]. Its application to understand the mechanism of interactions of site-specific binding proteins with DNA is illustrated in Fig. 4. This figure shows four frames (out of several hundred) spanning over 20 s in which the process of searching specific sites by site-specific EcoRII protein was directly visualized [28]. The initial state (5 s) is a complex with a small loop that gradually increases over time (10 s). After 15 s, the protein stops moving and binds to another specific DNA site, as indicated by DNA length measurements. The change in the loop length occurs over a period of about 10 s, covering a distance of about 300 bp (102 nm) until the EcoRII complex stops at another recognition site, which corresponds to a rate of about 30 bp/s (10.2 nm/s). These data suggest that EcoRII binds to one recognition site and searches for another site by threading the DNA filament through the complex until the enzyme finds the second recognition site, upon which it forms a stable synaptic complex.

1.4 Sample Preparation Approaches for AFM of DNA and Protein–DNA Complexes

The scanning tip can move or even sweep the samples that are weakly bound to the surface. Ignoring the sweeping effect led to a number of scanning artifacts identified in early attempts to image DNA with scanning tunneling microscope (STM), a predecessor of AFM [29–32]. Therefore, the sample preparation procedure was emphasized in AFM studies of DNA and protein–DNA complexes. The first results revealing reliable AFM images of long DNA molecules were reported in the early 1990s when a number of sample preparation methods were developed [33, 34]. The laboratory of C. Bustamante [34] implemented the method of mica cationic treatment [35]. In this approach, the mica surface is treated with Mg^{2+} to increase the affinity of the negatively charged mica surface to DNA. Other metal

cations such as Co^{2+}, La^{3+}, and Zr^{4+} can be used for mica pretreatment to obtain images of DNA [36]. Later, experiments showed that pretreatment of mica with cations was not necessary [37–40], as DNA adheres if Mg^{2+} cations are present in the buffer. In the laboratory of Z. Shao, an approach utilizing a modification of the well-known electron microscopic procedure for imaging DNA was developed [41, 42]. This method involves spreading DNA onto a carbon-coated mica substrate following cytochrome *c* denaturation at the air–water interface. Among these methods, the cation-assisted technique has become the most widely used due to the simplicity of sample preparation. However, the requirement for multivalent cations is mandatory and therefore limits the range of experimental conditions to buffers with a defined concentration of cations. Alternatives to these techniques were methods utilizing mica functionalization (reviewed in refs. [19, 43–45]). A weak cationic surface is obtained if (3-aminopropyl) triethoxysilane (APTES) is used to functionalize the mica surface with amino groups (AP-mica). As a result, functionalized surfaces remain positively charged at pH below p K_a values (p K_a = 10.4) and are capable of binding to negatively charged DNA in the pH range of stable DNA duplexes. Hydrolysis and aggregation of APTES is a complication associated with this technique.

An alternative to this technique is a more hydrolytically stable silatrane reagent, 1-(3-aminopropyl) silatrane (APS). Slow hydrolysis of the silatrane moiety allows avoidance of clumping and enables a smooth modification of the surface with amino groups achieving results similar to APTES vapor treatment. The schematics for the APS chemical formula and its reaction with the mica surface are shown in Fig. 5. The reaction with the surface (Fig. 5a) proceeds through several steps with eventual loss of the triethanolamine molecule and covalent attachment of the 3-aminopropyl siloxane group to the mica. The silatrane can be bound to several adjacent OH groups and these arrangements are shown in Fig. 5b. Both AP-mica and APS-mica methods are robust and work reproducibly in various topographic studies involving DNA [10, 12, 14, 44, 46–55]. Additionally, the APS-mica methodology works reliably for force spectroscopy AFM applications [56–60]. The sections below provide specific details related to the preparation of APS-mica surfaces for AFM imaging, including the procedure for the synthesis of the APS reagent.

2 Materials

2.1 General Equipment, Solutions, and Supplies

1. A vacuum cabinet or desiccator for storing samples. A Gravity Convention Utility Oven (VWR) is recommended.
2. Plastic tubes, 15 mL.
3. Eppendorf tubes, 1.5 mL.
4. Plastic cuvettes.
5. Scissors.
6. Razor blade.
7. 2 L glass desiccators and vacuum line (50 mmHg is sufficient).

8. Pipettes with plastic tips for rinsing the samples.
9. Tweezers.
10. Gas tank with clean argon gas. Nitrogen gas can be used as well.
11. Mica substrate. Any type of commercially available mica sheets (green or ruby mica) can be used. Asheville-Schoonmaker Mica Co (Newport News, VA) supplies thick and large (more than 5 cm× 7 cm) sheets (Grade 1) suitable for making substrates of different thickness and size.
12. Deionized water filtered through 0.2 μm filter for mica functionalization and AFM sample preparation.
13. Solution of sodium hydroxide in methanol (2 mg/mL).
14. AFM tips. For imaging in air, any type of tip with a spring constant of approximately 40 N/m and a resonance frequency between 300 and 340 kHz can be used. For example, Olympus silicon probes (Asylum Research, Santa Barbara, CA), with a spring constant of 40 N/m and a 300 kHz resonance frequency in air, work reliably in the tapping/oscillating mode for imaging in air. Probes with similar characteristics are currently manufactured by a large number of other vendors.
15. For imaging in liquid with a regular AFM, $Si_3 N_4$, 100-μm-long probes (SNL, Bruker Nano/Veeco, Santa Barbara, CA) with a spring constant of approximately 0.06 N/m and a resonance frequency around 7–10 kHz were used. Tips with similar characteristics from other vendors are available.
16. AFM instrument. Many instruments from different vendors are currently available. The authors used MM AFM (Bruker Nano, Santa Barbara, CA) for years; therefore, the instrument-related specifics are described for this particular instrument.

3 Methods

3.1 Synthesis of Aminopropyl Silatrane (APS)

The procedure described below is a modified version of our previously published method [45]. We tested and verified that sodium hydroxide can be used as a catalyst instead of the previously recommended sodium metal. We also found that reproducibility and chance of crystallization after reaction completion substantially improve when precise stoichiometric amounts of triethanolamine and (3-aminopropyl) triethoxysilane are used. For this purpose, we recommend using a precision balance rather than graduated cylinders for measuring the volumes of these liquid reagents. The reaction is essentially quantitative and is described by the schematic in Fig. 5a (*see* Notes 1 and [2] for additional information).

1. Prepare the 2 mg/mL by adding sodium hydroxide granules to the calculated amount of methanol and stirring until all sodium hydroxide is completely dissolved. Sonication or moderate heat can accelerate the process (*Caution* :

[1]Although APS synthesis can be performed in a round-bottom flask under vacuum with manual stirring, the best results were obtained using a rotary evaporator.
[2]APS is typically crystallized as described above; however, both crystallized and noncrystallized reagents performed equally well in AFM experiments.

sodium hydroxide solid and solutions can cause burns to the eyes and skin. Do not heat a closed vial.).

2. Add triethanolamine (14.92 g, 0.1 M) to a 250 mL round-bottom flask followed by 2 mL of sodium hydroxide solution in methanol (2 mg/mL). A precise equivalent amount of (3-aminopropyl) triethoxysilane (APTES; 22.14 g, 0.1 M) is measured in a separate flask and added to the reaction mixture. Complete transfer of the reagent is assured by washing the flask with two portions of methanol (2 × 10 mL) and adding the methanol washes to the reaction mixture.

3. Place the reaction flask on a rotary evaporator (*see* Note 1); methanol is evaporated at 40 °C under a moderate vacuum (100 Torr). This part of the process takes approximately 10 min.

4. Lower the vacuum gradually to 1 Torr; raise the temperature of the water bath to 60 °C. Make sure that the flask is rotated constantly and the vacuum is applied slowly to avoid bumping. Ethanol that forms in the reaction is evaporated off. At the end of the reaction, the product solidifies to a crystalline mass (*see* Note 2). The crystallization starts spontaneously after approximately 30 min. The product forms quantitatively; the yield is 23.22 g of colorless solid material. The melting point is 86–90 °C. We have shown that this product is suitable for the preparation of APS mica. Traces of sodium hydroxide in the product do not affect the performance or pH of solutions for AFM.

5. Transfer of the crude solid product from the reaction flask into a storage container may be difficult due to its hardness. To simplify handling of the material and improve its purity, we recommend the following crystallization method.

6. Save a small portion of the solid product (10–20 mg) for seeding crystallization. The rest of the solid product is dissolved in hot methanol (15 mL) and diluted with toluene (150 mL). The mixture is partially evaporated to approximately 1/2 of the volume. If the product does not crystallize during evaporation, the solution is seeded with a small portion of the saved crude solid product, stirred and crystallized. Crystallization can be accelerated by sonication or stirring and spreading the seed crystals with a spatula.

7. Cool the mixture by placing the flask on ice. Crystals of the product form a slurry.

8. The solid material is collected by filtration using a medium porosity sintered-glass filter and vacuum suction, washed with two 20 mL portions of ice-cold toluene, and dried under a vacuum. *Comment*: avoid prolonged suction of air through the solid product after the filtration and wash steps. The solid product can absorb moisture from the air and melt.

9. The final product (11.3 g) is a colorless powder. APS prepared and purified by this method has a melting point (m.p.) of 91–94 °C (open capillary tube); literature m.p. 87.2–87.9 °C (sealed capillary tube) (US Patent 3,118,921). ^{1}H NMR (DMSO-d_6), ppm: 0.08–0.14 (2H, m, $SiCH_2$); 1.1 (2H, br. s, NH_2); 1.28–1.37 (2H, m, CH_2);

2.37 (2H, t J = 7.2 Hz, NCH_2); 2.77 (6H, t J = 5.9 Hz, NCH_2); 3.59 (6H, t J = 5.9 Hz, OCH_2).

10. The APS reagent should be stored refrigerated over a desiccant. The reagent tested with AFM demonstrated good performance after 3 years of storage under these conditions.

3.2 Mica Functionalization with APS

1. Prepare a 50 mM APS stock solution in deionized water and store it in the refrigerator. The stock solution can be kept for more than a year at 4 °C (*see* Note 3).
2. Dissolve the APS from the stock in a 1:300 ratio in water (e.g., 50 μL of the stock to 15 mL deionized H_2O) to make the working APS solution for mica modification; it can be stored at room temperature for several days.
3. Cut both sides of the mica sheets to make strips of the required size (typically 1.2 cm × 3 cm) and cleave the strips with a razor blade, or scotch tape to make them as thin as 0.05–0.1 mm. Do not touch the cleaved mica surface (*see* Note 4).
4. Place the mica strips in appropriate plastic tubes or cuvettes.
5. Pour the working APS solution over the mica strip to cover it completely.
6. Leave the tubes/cuvettes on the bench for 30 min.
7. After 30 min, discard the APS solution.
8. Rinse both sides of the mica with deionized water.
9. Completely dry both sides of the mica strips under argon flow. Put the dry mica strips into the clean dry cuvette for storage (*see* Note 5). The strips are ready for sample preparation. Additional storage in a vacuum for 1–2 h is recommended when the environment is humid.

3.3 Sample Preparations for AFM Imaging in Air

The sections below describe the procedures for the preparation of samples of DNA or protein–DNA complexes for AFM imaging (*see* Note 9).

---

[3]It is recommended to aliquot the APS stock solution (1 mL). The aliquots can be stored in a refrigerator (4 °C) for more than a year.
[4]Depending on the size of the mica strip, plastic disposable 3 mL cuvettes or plastic 15 mL tubes are suitable for the mica functionalization process and storage.
[5]As prepared, the APS-mica sheets can be stored dry (plastic tubes or cuvettes) in the argon atmosphere for at least a week.
[9]*Alternative procedures for AFM sample preparation*. This paper describes protocols for substrate preparation, utilizing chemical functionalization of mica, and outlines the major features of these methods. Other methods have been developed, including the method based on using multivalent metal cations to analyze DNA by AFM [34, 36, 65]. This approach is appealing due to the simplicity of the procedure, but the mandatory requirement for the presence of multivalent metal ions limits the use of the cation-assisted method. Other problems with this method were identified and discussed in refs. [18, 44]. On the contrary, the AP-mica and APS-mica procedures are much more flexible. They do not require additional ions for DNA immobilization, and they function in a broad range of ionic strengths, pH, and temperatures. Alternative AFM sample preparation techniques do not have these features.

3.3.1 Droplet Procedure

1. Prepare the solution of the sample (DNA, RNA, protein–DNA complex) in an appropriate buffer. The DNA concentration should be between 0.8 and 0.01 μg/mL, depending on the size of the molecules. The concentration 0.2 μg/mL is recommended for PUC plasmid DNA, and higher concentrations (0.8 μg/mL) are recommended for smaller 1 kb DNA fragments. Concentrations as low as 0.01 μg/mL were used for imaging lambda DNA (~50 Kb) [61].
2. Cut the APS-mica substrates to a desired size (1 cm × 1 cm squares for the MultiMode AFM instrument) and place 5–10 μl of the solution in the middle of the substrate for 2 min.
3. Rinse the sample thoroughly with deionized water (2–3 mL per sample) to remove all buffer components. 5 mL or 10 mL plastic syringes are useful for rinsing. Attach an appropriate plastic tip instead of a metal needle.
4. Dry the sample with clean argon gas. Additional drying of samples for an hour or two prior to imaging is recommended to ensure low tip adhesion. The samples can be stored in vacuum cabinets or desiccators filled with argon. The samples, as prepared, can be imaged many times provided that after imaging they are stored as described. Their shelf life is more than a month.

3.3.2 The Immersion Procedure—This procedure is recommended if the deposition should be performed at strictly controlled temperature conditions (e.g., 0 °C or elevated temperatures).

1. Prepare the solution (DNA, RNA, nucleoprotein complexes) in an appropriate tube and preincubate it for 10–20 min to allow the temperature to equilibrate. The recommended concentration of DNA is between 0.8 and 0.01 μg/mL, depending on the DNA size (*see* Subheading 3.3.1, **step 1**). (*See* also Notes 6 and [7]). Immerse a piece of functionalized mica into the tube and leave it for a defined time (2–10 min) to allow the sample to adhere to the surface.
2. Remove the mica strip, rinse with water thoroughly, and dry under argon flow as described above. The sample is then ready for imaging; however, it is recommended that the specimen be stored in a vacuum cabinet under argon for an hour to allow optimum sample drying.

Two AFM microscopes, the MultiMode AFM system (Bruker Nano/Veeco, Santa Barbara, CA) and the MFP3 (Asylum Research, Santa Barbara, CA), were our primary instruments. However, the procedures described below are general and can be adapted with minimal adjustments to any AFM instrument (*see* Note 8).

[6]DNA concentration. This parameter depends on the length of the molecules. If the molecules are as small as several hundred base pairs, approximately 0.5–1 μg/mL is recommended to avoid intermolecular crossing. However, lower DNA concentrations are recommended for longer DNA molecules. For example, ~0.01 μg/mL of lambda DNA (~48 kB) allowed us to image individual long DNA molecules without overlap [61].

[7]DNA preparation. A very small amount of DNA is required to prepare the samples by the droplet procedure. Typically, 10 ng of DNA is sufficient to image plasmid DNA (~3Kb long). Due to the fact that one band of DNA in agarose gels usually contains 100 ng of DNA, DNA extracted from several bands is sufficient for the preparation of several samples. The gel purification procedure described in refs. [63, 64] produces pure samples.

3.4 AFM Imaging

This section describes the AFM imaging procedures for imaging dried and wet samples (*see* Note 9).

3.4.1 AFM Imaging in Air—AFM tips—*see* Subheading 2.1 for the probes specifics.

1. Mount the sample prepared at step 4 onto the AFM stage.
2. Tune the AFM probe to find the resonance frequency corresponding to the AFM probe.
3. Adjust the drive amplitude. For the MultiMode AFM, 6–8 mV is typical.
4. Set the image size to 100 nm × 100 nm and start approaching the surface.
5. Gradually reduce the set point until the surface of the sample is clearly seen. Increase the scan size and acquire the images.

Typical AFM images of DNA obtained with the use of the functionalized procedures are shown in Fig. 3. These images highlight a number of important features of the AP- and APS-mica procedures. First, the background is smooth, enabling unambiguous visualization of DNA [16, 62]. Second, the concentration of DNA was adjusted in such a way that the molecules are spread over the surface with no overlap. Third, various protein–DNA complexes were visualized. The buffer composition is not critical for both procedures, and this property was critical to image protein–DNA complexes differing broadly in their buffer composition.

3.4.2 Imaging in Liquid—The protocols described below were developed with the use of MultiMode AFM (Bruker Nano/Veeco), but they can be adapted to any type of AFM. Selection of the probe— *see* Subheading 2.1 for specifics.

1. Mount the tip on the tip holder.
2. Place the stage with the attached APS-mica substrate on the instrument stage. It is a scanner for the MM AFM instrument. Mica pieces 1 cm × 1 cm work well for MM AFM. Double stick tape can be used to attach the modified mica substrate to the metal discs. However, if glue is used, glue the mica and cleave it prior to the functionalization step. The glue vapors react with the mica surface preventing its reaction with APS.
3. Use the video camera to find the tip and approach the surface manually, leaving a 500–100 μm gap between the tip and the surface.
4. Place a droplet of the prepared sample solution and readjust the spot position. The spot changes due to the difference in the refractive indexes of air and water. For

[8]Imaging conditions. It is recommended to operate the instrument at the lowest possible drive amplitude. This recommendation is based on the following considerations. The oscillating tip transfers a large amount of energy to the sample. According to [62], the total energy applied to the sample by the oscillating tip can be as high as 10^{-16}–10^{-17} J at 30 nm amplitude of oscillation. However, this value is almost three orders of magnitude lower if the microscope is operated at an amplitude as low as ~3 nm. These imaging conditions allow the dragging effect of the tip to be minimized, prevent damaging the tip, enable the acquisition of high contrast images, and facilitate the study of dynamic processes, such as segmental DNA mobility or protein–DNA interactions (reviewed in ref. [19]).

MM AFM, 50 μL of the solution is sufficient to fill the gap. Note that due to the elevated hydrophobicity of APS mica compared to bare mica, the spot does not spread; therefore, an additional O-ring is not required to keep the solution in place.

5. Find a resonance peak. Typically it is quite a broad peak, around 7–10 kHz, for the MultiMode AFM instrument. Follow the recommendations given in the manual for how to find the peak in fluid.

6. Start the computer controlled approach. Operate with the setpoint voltage and drive amplitude parameters to improve the quality of images. Minimize the drive amplitude. The number varies from tip to tip, but an amplitude as low as 10 nm or less and a scanning rate of approximately 2 Hz provide better quality pictures.

Dried samples can be imaged in aqueous solutions as well. In this case, the procedure is similar, but instead of using the sample solution at **step 4**, a buffer solution is placed on top of the substrate.

Acknowledgments

The authors thank the members of the Lyubchenko lab for their contribution to different parts of the paper. The work is supported by grants to Y.L.L. from the DOE (DE-FG02-08ER64579), NIH (P01 GM091743, 5 R01 GM096039-02), NSF (EPS—1004094), and the Nebraska Research Initiative (NRI).

References

1. Binnig G, Rohrer H, Gerber C, et al. Surface studies by scanning tunneling microscopy. Phys Rev Lett. 1982; 49:57–61.
2. Binning G, Rohrer H. Scanning tunneling microscopy. Helvetica Phys Acta. 1982; 55:726–735.
3. Binnig G, Quate CF, Gerber C. Atomic force microscope. Phys Rev Lett. 1986; 56:930–933. [PubMed: 10033323]
4. Ohnesorge F, Binnig G. True atomic resolution by atomic force microscopy through repulsive and attractive forces. Science. 1993; 260:1451–1456. [PubMed: 17739801]
5. Gross L, Mohn F, Moll N, et al. Bondorder discrimination by atomic force microscopy. Science. 2012; 337:1326–1329. [PubMed: 22984067]
6. Martin Y, Williams CC, Wickramasinghe HK. Atomic force microscope-force mapping and profiling on a sub 100-A scale. J Appl Phys. 1987; 61:4723–4729.
7. Zhong Q, Inniss D, Kjoller K, et al. Fractured polymer/silica fiber surface studied by tapping mode atomic force microscopy. Surf Sci Lett. 1993; 290:L688–L692.
8. Wickramasinghe HK. Development of the technology and applications of the scanning probe microscope. Microsc Anal. 2012; 26:27–30.
9. Vetcher AA, Lushnikov AY, Navarra-Madsen J, et al. DNA topology and geometry in Flp and Cre recombination. J Mol Biol. 2006; 357:1089–1104. [PubMed: 16483600]
10. Lushnikov AY, Potaman VN, Lyubchenko YL. Site-specific labeling of supercoiled DNA. Nucleic Acids Res. 2006; 34:e111, 111–117. [PubMed: 16963492]
11. Soyfer, VN.; Potaman, VN. Triple-helical nucleic acids. Springer; New York: 1996.
12. Tiner WJ Sr, Potaman VN, Sinden RR, et al. The structure of intramolecular triplex DNA: atomic force microscopy study. J Mol Biol. 2001; 314:353–357. [PubMed: 11846549]
13. Potaman VN, Ussery DW, Sinden RR. Formation of a combined H-DNA/open TATA box structure in the promoter sequence of the human Na, K-ATPase alpha2 gene. J Biol Chem. 1996; 271:13441–13447. [PubMed: 8662935]

14. Kato M, McAllister CJ, Hokabe S, et al. Structural heterogeneity of pyrimidine/purine-biased DNA sequence analyzed by atomic force microscopy. Eur J Biochem. 2002; 269:3632–3636. [PubMed: 12153559]
15. Shlyakhtenko LS, Hsieh P, Grigoriev M. A cruciform structural transition provides a molecular switch for chromosome structure and dynamics. J Mol Biol. 2000; 296:1169–1173. [PubMed: 10698623]
16. Lyubchenko YL, Jacobs BL, Lindsay SM, et al. Atomic force microscopy of nucleoprotein complexes. Scanning Microsc. 1995; 9:705–724. discussion 724–707. [PubMed: 7501986]
17. Lyubchenko YL, Shlyakhtenko LS. AFM for analysis of structure and dynamics of DNA and protein-DNA complexes. Methods. 2009; 47:206–213. [PubMed: 18835446]
18. Lyubchenko YL. Preparation of DNA and nucleoprotein samples for AFM imaging. Micron. 2011; 42:196–206. [PubMed: 20864349]
19. Lyubchenko YL, Shlyakhtenko LS, Ando T. Imaging of nucleic acids with atomic force microscopy. Methods. 2011; 54:274–283. [PubMed: 21310240]
20. Ando T, Uchihashi T, Kodera N, et al. High-speed AFM and nano-visualization of biomolecular processes. Pflugers Arch. 2008; 456:211–225. [PubMed: 18157545]
21. Ando T, Uchihashi T, Kodera N, et al. High-speed atomic force microscopy for observing dynamic biomolecular processes. J Mol Recognit. 2007; 20:448–458. [PubMed: 17902097]
22. Ando T, Kodera N, Takai E, et al. A high-speed atomic force microscope for studying biological macromolecules. Proc Natl Acad Sci USA. 2001; 98:12468–12472. [PubMed: 11592975]
23. Suzuki Y, Higuchi Y, Hizume K, et al. Molecular dynamics of DNA and nucleosomes in solution studied by fast-scanning atomic force microscopy. Ultramicroscopy. 2010; 110:682–688. [PubMed: 20236766]
24. Suzuki Y, Gilmore JL, Yoshimura SH, et al. Visual analysis of concerted cleavage by Type IIF restriction enzyme SfiI in subsecond time region. Biophys J. 2011; 101:2992–2998. [PubMed: 22208198]
25. Miyagi A, Ando T, Lyubchenko YL. Dynamics of nucleosomes assessed with time-lapse high-speed atomic force microscopy. Biochemistry. 2011; 50:7901–7908. [PubMed: 21846149]
26. Shlyakhtenko LS, Lushnikov AY, Miyagi A, et al. Specificity of binding of single-stranded DNA-binding protein to its target. Biochemistry. 2012; 51:1500–1509. [PubMed: 22304461]
27. Shlyakhtenko LS, Lushnikov AY, Miyagi A, et al. Nanoscale structure and dynamics of ABOBEC3G complexes with single-stranded DNA. Biochemistry. 2012; 51:6432–6440. [PubMed: 22809226]
28. Gilmore JL, Suzuki Y, Tamulaitis G, et al. Single-molecule dynamics of the DNA-EcoRII protein complexes revealed with highspeed atomic force microscopy. Biochemistry. 2009; 48:10492–10498. [PubMed: 19788335]
29. Beebe TP Jr, Wilson TE, Ogletree DF, et al. Direct observation of native DNA structures with the scanning tunneling microscope. Science. 1989; 243:370–372. [PubMed: 2911747]
30. Arscott PG, Lee G, Bloomfield VA, et al. Scanning tunnelling microscopy of Z-DNA. Nature. 1989; 339:484–486. [PubMed: 2725682]
31. Lee G, Arscott PG, Bloomfield VA, et al. Scanning tunneling microscopy of nucleic acids. Science. 1989; 244:475–477. [PubMed: 2470146]
32. Clemmer CR, Beebe TP Jr. Graphite: a mimic for DNA and other biomolecules in scanning tunneling microscope studies. Science. 1991; 251:640–642. [PubMed: 1992517]
33. Lyubchenko YL, Gall AA, Shlyakhtenko LS, et al. Atomic force microscopy imaging of double stranded DNA and RNA. J Biomol Struct Dyn. 1992; 10:589–606. [PubMed: 1492926]
34. Bustamante C, Vesenka J, Tang CL, et al. Circular DNA molecules imaged in air by scanning force microscopy. Biochemistry. 1992; 31:22–26. [PubMed: 1310032]
35. Brack C. DNA electron microscopy. CRC Crit Rev Biochem. 1981; 10:113–169. [PubMed: 6163590]
36. Thundat T, Allison DP, Warmack RJ, et al. Atomic force microscopy of DNA on mica and chemically modified mica. Scanning Microsc. 1992; 6:911–918. [PubMed: 1295085]

37. Hansma HG, Vesenka J, Siegerist C, et al. Reproducible imaging and dissection of plasmid DNA under liquid with the atomic force microscope. Science. 1992; 256:1180–1184. [PubMed: 1589799]
38. Bezanilla M, Manne S, Laney DE, et al. Adsorption of DNA to Mica, silylated mica, and minerals: characterization by Atomic Force Microscopy. Langmuir. 1995; 11:655–659.
39. Bustamante C, Rivetti C. Visualizing protein-nucleic acid interactions on a large scale with the scanning force microscope. Annu Rev Biophys Biomol Struct. 1996; 25:395–429. [PubMed: 8800476]
40. Bustamante C, Rivetti C, Keller DJ. Scanning force microscopy under aqueous solutions. Curr Opin Struct Biol. 1997; 7:709–716. [PubMed: 9345631]
41. Yang J, Takeyasu K, Shao Z. Atomic force microscopy of DNA molecules. FEBS Lett. 1992; 301:173–176. [PubMed: 1314740]
42. Yang J, Tamm LK, Tillack TW, et al. New approach for atomic force microscopy of membrane proteins. The imaging of cholera toxin. J Mol Biol. 1993; 229:286–290. [PubMed: 8429547]
43. Lyubchenko YL, Gall AA, Shlyakhtenko LS. Atomic force microscopy of DNA and protein-DNA complexes using functionalized mica substrates. Methods Mol Biol. 2001; 148:569–578. [PubMed: 11357614]
44. Lyubchenko YL. DNA structure and dynamics: an atomic force microscopy study. Cell Biochem Biophys. 2004; 41:75–98. [PubMed: 15371641]
45. Lyubchenko YL, Shlyakhtenko LS, Gall AA. Atomic force microscopy imaging and probing of DNA, proteins, and protein DNA complexes: silatrane surface chemistry. Methods Mol Biol. 2009; 543:337–351. [PubMed: 19378175]
46. Shlyakhtenko LS, Potaman VN, Sinden RR, et al. Structure and dynamics of three-way DNA junctions: atomic force microscopy studies. Nucleic Acids Res. 2000; 28:3472–3477. [PubMed: 10982865]
47. Lyubchenko YL, Shlyakhtenko LS, Potaman VP, et al. Global and local DNA structure and dynamics. Single molecule studies with AFM. Microsc Microanal. 2002; 8:170–171. [PubMed: 12539787]
48. Yodh JG, Woodbury N, Shlyakhtenko L, et al. Mapping nucleosome locations on the 208–12 by AFM provides clear evidence for cooperativity in array occupation. Biochemistry. 2002; 41:3565–3574. [PubMed: 11888272]
49. Kato M, Hokabe S, Itakura S, et al. Interarm interaction of DNA cruciform forming at a short inverted repeat sequence. Biophys J. 2003; 85:402–408. [PubMed: 12829494]
50. Potaman VN, Bissler JJ, Hashem VI, et al. Unpaired structures in SCA10 (ATTCT)n.(AGAAT)n repeats. J Mol Biol. 2003; 326:1095–1111. [PubMed: 12589756]
51. Shlyakhtenko LS, Gall AA, Filonov A, et al. Silatrane-based surface chemistry for immobilization of DNA, protein-DNA complexes and other biological materials. Ultramicroscopy. 2003; 97:279–287. [PubMed: 12801681]
52. Lushnikov AY, Brown BA 2nd, Oussatcheva EA, et al. Interaction of the Zalpha domain of human ADAR1 with a negatively supercoiled plasmid visualized by atomic force microscopy. Nucleic Acids Res. 2004; 32:4704–4712. [PubMed: 15342791]
53. Dahlgren PR, Karymov MA, Bankston J, et al. Atomic force microscopy analysis of the Huntington protein nanofibril formation. Dis Mon. 2005; 51:374–385. [PubMed: 16242522]
54. Lonskaya I, Potaman VN, Shlyakhtenko LS, et al. Regulation of poly(ADP-ribose) polymerase-1 by DNA structure-specific binding. J Biol Chem. 2005; 280:17076–17083. [PubMed: 15737996]
55. Lushnikov AY, Potaman VN, Oussatcheva EA, et al. DNA strand arrangement within the SfiI-DNA complex: atomic force microscopy analysis. Biochemistry. 2006; 45:152–158. [PubMed: 16388590]
56. McAllister C, Karymov MA, Kawano Y, et al. Protein interactions and misfolding analyzed by AFM force Spectroscopy. J Mol Biol. 2005; 354:1028–1042. [PubMed: 16290901]
57. Kransnoslobodtsev AV, Shlyakhtenko LS, Ukraintsev E, et al. Nanomedicine and protein misfolding diseases. Nanomedicine. 2005; 1:300–305. [PubMed: 16467913]
58. Lyubchenko YL, Sherman S, Shlyakhtenko LS, et al. Nanoimaging for protein misfolding and related diseases. J Cell Biochem. 2006; 99:53–70.

59. Krasnoslobodtsev AV, Shlyakhtenko LS, Lyubchenko YL. Probing interactions within the synaptic DNA-SfiI complex by AFM force spectroscopy. J Mol Biol. 2007; 365:1407–1418. [PubMed: 17125791]

60. Shlyakhtenko LS, Yuan B, Emadi S, et al. Single-molecule selection and recovery of structure-specific antibodies using atomic force microscopy. Nanomedicine. 2007; 3:192–197. [PubMed: 17662669]

61. Lyubchenko Y, Shlyakhtenko L, Harrington R, et al. Atomic force microscopy of long DNA: imaging in air and under water. Proc Natl Acad Sci USA. 1993; 90:2137–2140. [PubMed: 8460119]

62. Lyubchenko YL, Shlyakhtenko LS. Visualization of supercoiled DNA with atomic force microscopy *in situ*. Proc Natl Acad Sci USA. 1997; 94:496–501. [PubMed: 9012812]

63. Lushnikov AY, Bogdanov A, Lyubchenko YL. DNA recombination: holliday junctions dynamics and branch migration. J Biol Chem. 2003; 278:43130–43134. [PubMed: 12949070]

64. Shlyakhtenko LS, Gilmore J, Kriatchko AN, et al. Molecular mechanism underlying RAG1/RAG2 synaptic complex formation. J Biol Chem. 2009; 284:20956–20965. [PubMed: 19502597]

65. Vesenka J, Guthold M, Tang CL, et al. Substrate preparation for reliable imaging of DNA molecules with the scanning force microscope. Ultramicroscopy. 1992:42–44. 1243–1249.

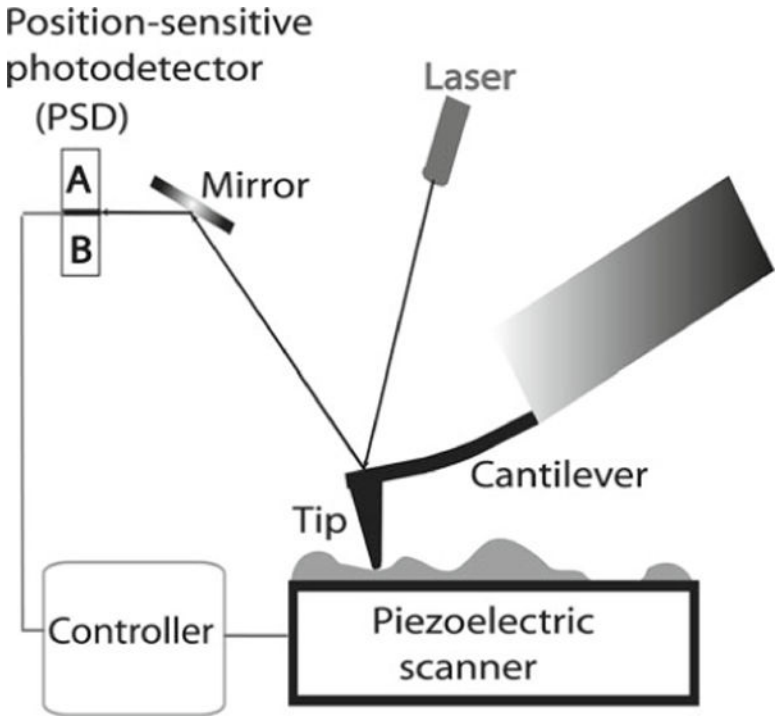

Fig. 1.

Schematic explaining the principles of AFM. The position of the tip relative to the sample is controlled by a piezoelectric scanner. The vertical displacement of the tip during scanning is detected using the optical lever principle, in which the position of the light spot on the PSD is measured

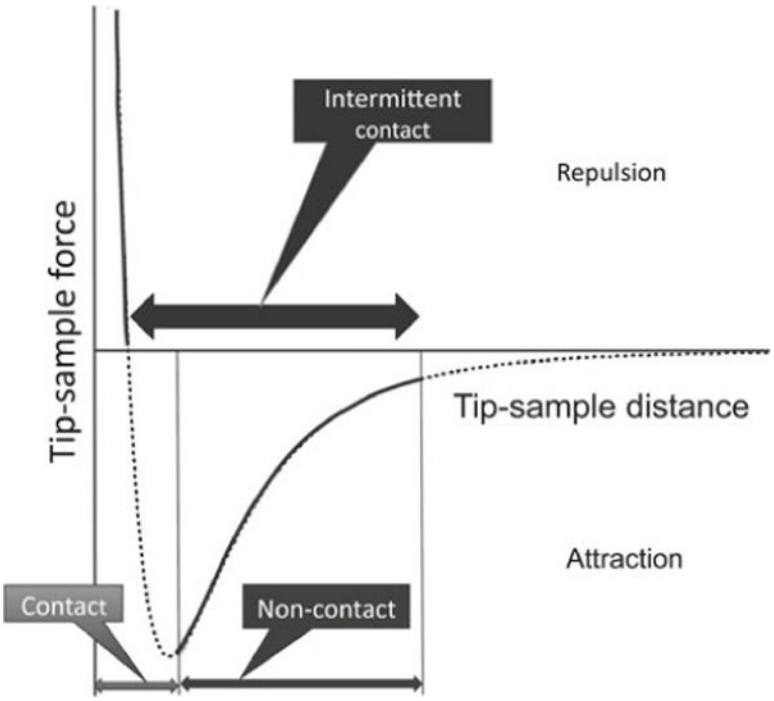

Fig. 2.

Schematic explaining the different modes of AFM operation. The curve in the schematic shows the change of the tip–sample interaction energy dependent on the distance between the apex of the tip and the sample

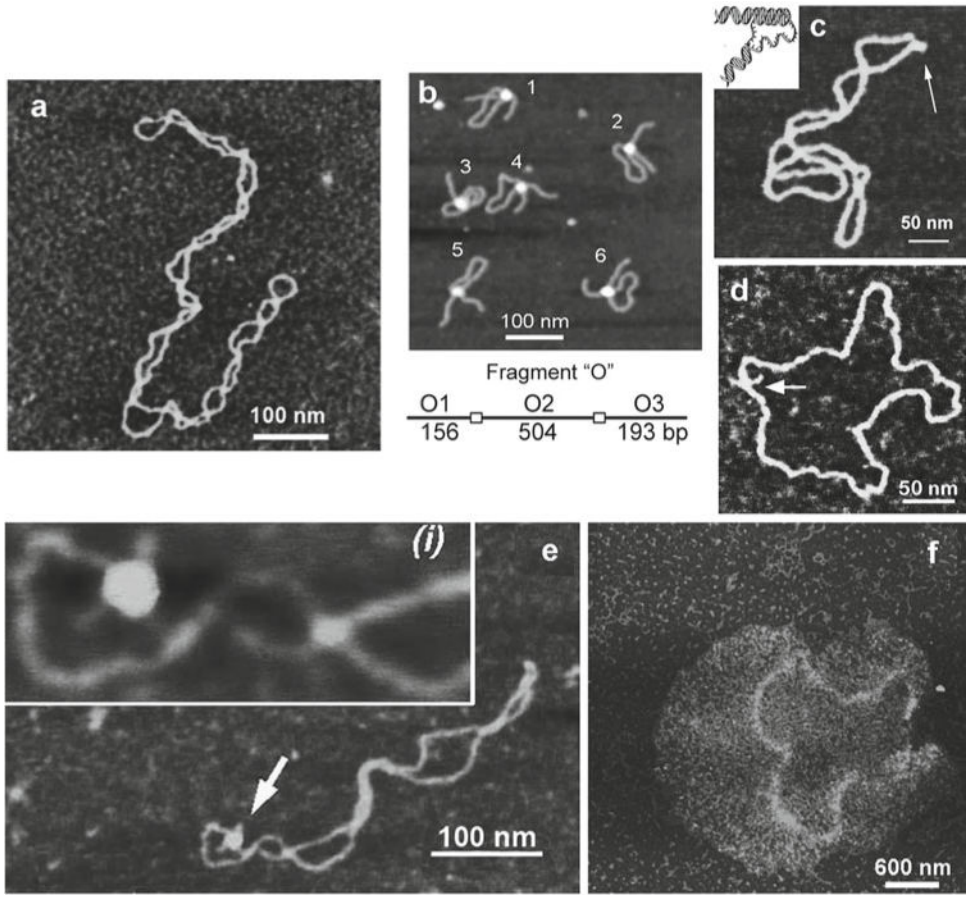

Fig. 3.

A set of AFM images of various samples. Plate (**a**) shows the AFM image of supercoiled plasmid DNA. Plate (**b**) shows AFM images of complexes of DNA with Sfil restriction enzyme. The schematic in (**b**) explains the design of the DNA construct; positions of the Sfil binding sites are indicated with *squares* and the *numbers* are shown in base pairs (bp). More information and animated images can be found in ref. [55]. The figure was reproduced from Lushnikov [55] with the permission of the American Chemical Society. Plate (**c**) shows the image of plasmid DNA with H-form DNA appearing as a clear-cut protrusion on the image. pCW2966 contains a 46 bp mirror repeat forming H-DNA at acidic pH. A sharp kink at the base of the thick protrusion is indicated with an *arrow*. The *inset* shows the schematic for H-DNA structure. More information and animated images can be found in [12]. The figure was reproduced from Tiner et al. [12], with the permission of Elsevier. Plate (**d**) shows the image of circular pUC8F14C plasmid DNA containing a 106 bp inverted repeat forming cruciforms under appropriate supercoiling density. DNA with the cruciform protrusion is indicated with an *arrow*. Image (**e**) demonstrates the formation of complexes of the same plasmid DNA with RuvA protein (indicated with an *arrow*). *Inset* (**i**) is the higher-resolution image of the DNA segment with the bound protein. More information can be found in ref. [15]. The figure was reproduced from Shlyakhtenko et al. [15] with the permission from Elsevier. The images were acquired in air with MultiMode AFM operated with NanoScope IIId and IV controllers (Veeco)

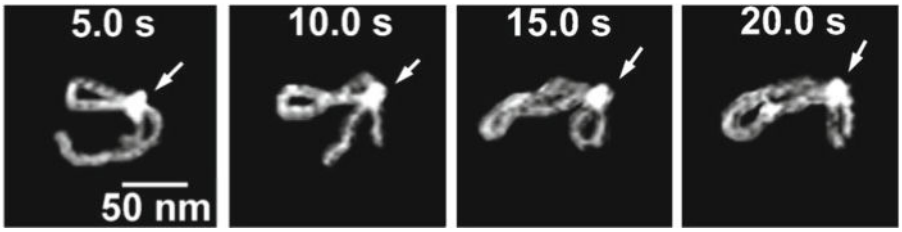

Fig. 4.

EcoRII translocation process analyzed by high-speed AFM. Four frames out of 40 frames total were taken over a time period of 20 s measured in 0.5 s intervals. In the first frame (5 s) the looped structure is formed, stabilized by the protein (indicated with an *arrow*) bound to two specific sites on the DNA. The following frames illustrate sliding of the protein along the DNA strand, leading to an increase in the loop size. The final image (20 s), in which a large loop is formed, corresponds to binding of the protein to two distant binding sites on the DNA substrate. More information and animated images can be found in ref. [28]. The modified figure was reproduced from Gilmore et al. [28], with the permission of the American Chemical Society

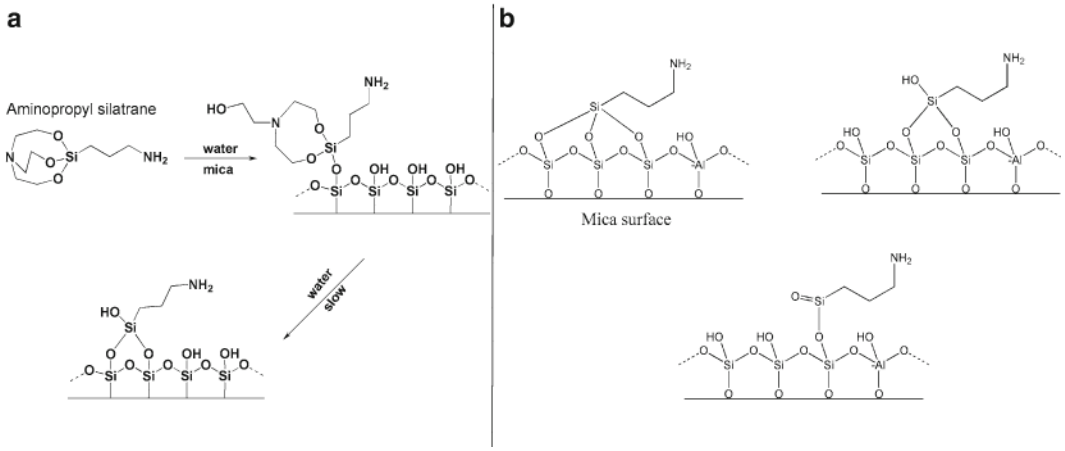

Fig. 5.

The reaction of aminopropyl silatrane (APS) with silicon surfaces. (**a**) Schematic for the reaction of APS with the hydroxyl groups (OH groups) on silicon surfaces. The OH groups on the mica surface formed spontaneously after cleavage. Initial and final stages of the reaction are shown. Note the last stage, exposure of APS-functionalized mica to water, leads to dissociation of triethanolamine yielding the stable product. (**b**) illustrates the reaction of APS with three, two, and single OH groups (from left to right). Mica contains Al atoms as shown in this scheme